

Peer Reviewed

Sunlight Driven Activated Carbon Modified BiVO₄ Photocatalyst for the Degradation of Rhodamine-B

Prabhavathy S · Arivuoli Dakshanamoorthy

Crystal Growth Centre, Anna University, Chennai, India.

ABSTRACT

An Efficient photocatalysts for environmental remediation have generated much interest in recent times with a significant emphasis on natural light source. In the present study, activated carbon (AC) incorporated BiVO₄ (BV) were synthesized using hydrothermal method and their photocatalytic properties were studied through the photodegradation of Rhodamine B (Rh-B) as a model pollutant under sunlight irradiation. The structural and morphological characteristics of BV and AC-BV nanoparticles have been ascertained, which reveals BV crystallizes in pure monoclinic phase at 120 °C, whereas the modification with AC leads to hexagonal shaped particles. In an effort to develop highly active visible light photocatalysts, small particle size, extended visible absorption in solar spectrum, narrow bandgap and increased surface area were achieved. The inclusion of AC into BV nanoparticles assists the bandgap tuning from 2.4 eV to 1.9 eV which effectively improves the visible light activity of BiVO₄. The AC-BV nanoparticles possess mesoporous structure with high surface area of 68.10 m²/g which is 9 times greater than that of BV nanoparticles (7.34 m²/g). The synthesized AC-BV nanoparticles degrade the pollutant about 98% within 60 minutes whereas BV nanoparticles degrade 47% at same condition. The influence of AC on BV triggers the rate of degradation, due to the narrow bandgap and porosity of the carbon. This study provides a promising photocatalyst to be used for treatment of effluents in large scale.

© 2021 JMSSE · INSCIENCEIN. All rights reserved

ARTICLE HISTORY

Received 27-07-2021

Revised 01-11-2021

Accepted 13-11-2021

Published 13-12-2021

KEYWORDS

BiVO₄

Activated Carbon

Visible Light

Photocatalysis

Dye Degradation

Introduction

Enormous release of dyes without further pre-treatment have not only polluted the water system upon all development is based, but have also posed a major threat to human life and various aquatic creatures [1]. The use of heterostructure for clean water and environmental remediation has gained more attention in recent times because of their efficient use of naturally available solar energy and an effective system to eliminate different hazardous substances [2]. In addition, photocatalysis method can lead fast and complete mineralization of contaminants without leaving harmful intermediates due to its enormous oxidising power and non-selective nature of the products produced in the process [3]. TiO₂ and ZnO are the common materials used for photocatalytic applications owing to their superior photocatalytic activity [4]. However, the main drawback of these photocatalysts is fascinated only ultraviolet portion of the solar spectrum [5].

A variety of semiconductors have been widely employed as photocatalysts by tuning its band position and make use of the solar spectrum effectively [6]. Over the past few years Bi based semiconductor plays a prime role of visible light photocatalysis due to its ionic conductivity, narrow bandgap etc., [7]. The lone pair of Bi (6s) orbital is combined with the orbital O (2p) to create a blue shift valence band (VB) that tends to reduce the bandgap [8]. Among the Bi based photocatalysts, BiVO₄ has recently been used for the photocatalytic degradation of organic compounds in waste water under the sunlight irradiation [9]. BiVO₄ may exist as three crystalline phases including, scheelite-monoclinic, zircon tetragonal and scheelite tetragonal [10]. It is well known that photocatalytic

properties always be subject to on its crystal structure [11]. The monoclinic structure of BiVO₄ shows stronger photocatalytic activity under visible light irradiation for its relatively small bandgap of 2.4 eV compared to other two tetragonal phases of bandgap energy of 2.9 eV [12]. Moreover, pure BiVO₄ has some limitations, low absorption rate of incident light, fast recombination of photo generated electrons, non-porous structure and low surface area [13-14].

It is an essential to strengthen its visible absorption range and restrict the recombination of photogenerated electrons and holes, in order to enhance the photocatalytic activity of BiVO₄ under visible light irradiation [15]. In this context, many efforts have been made, such as doping, adding bias energy and constructing heterostructure system [16]. The property of light reflection and scattering from the porous textured material are advantageous to light harvesting [17]. The combination of BiVO₄ with other porous supporting materials such as alumina, silica, zeolites, glass and activated carbon (AC) to improve the performance of light absorption and to suppress the recombination rate of charge carriers [18-19]. Due to porous structure, strong adsorption efficiency, structural stability, low cost and larger surface area of AC that facilitates a better adsorption of reactants, make it a promising material that supports photocatalytic process [20-21]. Thus, it allows the catalyst to absorb more dye molecules that further leads to a complete dye degradation [22]. A number of modifications have been reported by several authors on the photocatalyst surface using various supporting materials by different methods of synthesis, such as co-precipitation, sol-gel, solvothermal, hydrothermal and microwave synthesis [23]. It's quite well known that crystallinity is a key aspect in impacting the activity of photocatalysts. Hence, structure

controlled and highly crystalline nanoparticles have been prepared through hydrothermal method [24].

The present research explores the hydrothermally synthesized AC modified BiVO₄ photocatalyst. To enhance the photocatalytic efficiency, the band gap of BV nanoparticles can be narrowed by AC. The photocatalytic performance was assessed by photo degradation of Rh-B under sunlight irradiation. In addition, the pseudo-first-order kinetic model was used to examine the reaction mechanism of Rh-B on the surface of the photocatalyst. The recycling efficiency and long-term stability of the photocatalysts were also tested. The results provide insights into the synergistic influence of photocatalytic degradation using BiVO₄ on activated carbon. The results indicated that AC modified BiVO₄ can be used as ideal photocatalyst materials for rapid and high efficiency dye degradation.

Experimental

Materials & Methods

All the chemicals used were of analytical grade without further purification. Bismuth (III) Nitrate pentahydrate (Bi(NO₃)₃·5H₂O), Ammonium Metavanadate (NH₄VO₃), Polyvinyl Alcohol (PVA), Activated Carbon, Nitric Acid (HNO₃) were taken as starting materials. BiVO₄ nanoparticles were synthesized in a typical synthesis using hydrothermal method. 0.5g of PVA was dissolved in 25 ml of distilled water and stirred magnetically at 100°C until it turned to homogenous, following which 0.5g of activated carbon was added to it. To the above mixture 5 mM of NH₄VO₃ was added and allowed to stir for 30 minutes. Meanwhile, 5 mM of Bi(NO₃)₃·5H₂O was dissolved in 25 ml of aqueous HNO₃ solution separately. After 30 minutes of intense stirring, this mixture was added drop-wise to the above NH₄VO₃ solution under continuous stirring. The obtained clear precursor solution was then treated for 12 h in a sealed Teflon-lined stainless-steel autoclave under hydrothermal process at 180°C and allowed to cool down to room temperature. The precipitate was washed by centrifuge method for several times with distilled water and absolute ethanol. The final product dried for 8 h in vacuum oven at 100°C to eliminate the excess moisture content and reaction by-products. The same process followed for preparing of BiVO₄ nanoparticles without the inclusion of AC. The synthesized Bismuth Vanadate and activated carbon modified Bismuth Vanadate particles were labelled as BV and AC-BV respectively and represented as the same throughout the manuscript.

Characterization

The phase transitions of the synthesized samples were studied by powder X-ray diffraction using Cu-K α radiation [Panalytical X'Pert PRO; $\lambda=1.5406\text{\AA}$]. The detection range was from 15° to 65° with a step size of 0.02°. The Raman spectra measurements were detected by NXR FT-Raman Spectrometer. The morphology of the samples was investigated by Carl Zeiss MA15/EV018 Scanning Electron Microscope. Transmission Electron Microscopy (TEM) investigations were performed on Tecnai G² T20 operated at 200 kV. The surface chemical analysis of the samples was conducted X-ray photoelectron spectroscopy (XPS, PHI 5000 VersaProbe II, ULVAC-PHI Inc., USA) equipped with micro-focused (200 μm , 15 KV) monochromatic Al-K α X-Ray source ($h\nu = 1486.6\text{ eV}$). The Brunauer-Emmett-Teller (BET) specific surface area and Barrett-Joyner-Halenda

(BJH) pore size distribution of the samples were measured using MICROMERITICS ASAP 2020 POROSIMETER. The optical properties were evaluated using a diffuse reflectance UV JASCO UV-Vis spectrometer-V760 in the range of 200-800 nm. Photoluminescence (PL) measurement was conducted on Fluoromax-2, ISA; Jobin Yuvon-Spex.

Photocatalytic Experiment

The photocatalytic performance of BV and AC-BV nanoparticles was investigated by the degradation of Rh-B under sunlight. In a typical experiment, 10 mg of Rh-B dye powder was dissolved into 1000 ml of distilled water, in which 100 ml was used for the degradation experiment. 50 mg of BV photocatalyst was ultrasonically dispersed in 100 ml of dye solution. The suspension was stirred in the dark for 30 minutes, before irradiation to attain the adsorption/desorption equilibrium of dye on the surface of the catalyst. Then suspension was exposed to direct sunlight with an average intensity of 46 klux measured by Lux meter. At regular interval of every 15 minutes, 5 ml of dye solution was withdrawn and centrifuged in order to separate the sample and their corresponding absorption profile was measured. The same procedure followed to AC-BV nanoparticles to obtain comparative photocatalytic efficiency. The degradation efficiency was determined by the following equation [25].

$$\text{Deg \%} = \frac{C_0 - C_t}{C_0} \times 100 \quad (1)$$

Where C₀ is the initial concentration, C_t is the concentration at different time intervals.

Results and Discussion

Structural Analysis

Fig.1(a) shows the XRD patterns of AC, BV and AC-BV nanoparticles synthesized from hydrothermal process from which all the crystal planes and related 2 θ values were observed. Generally, the photocatalytic property of BiVO₄ is associated with crystalline phase; only the monoclinic scheelite structure has good photocatalytic activity [26]. Therefore, the objective of this synthesis is to produce more volume of monoclinic scheelite structured material.

All diffraction peaks correspond to the monoclinic scheelite structure of BiVO₄ with lattice constants a=5.195 \AA , b=11.701 \AA , c=5.092 \AA in accordance with the standard JCPDS No.14-0688. In addition, there were no diffraction peaks assigned to PVA indicating that, the introduction of PVA surfactant did not affect the lattice structure. In the AC-BV sample, at 2 θ of 24.4° confirmed the characteristic of the activated carbon matrix correlated with the diffraction of (002) plane. This often implies that the combination of AC with BiVO₄ did not impact the crystal phase of BiVO₄. Fig.1(b) shows the normalized intensity XRD plot of BiVO₄ and AC-BiVO₄ nanoparticles. The crystalline extent of AC is significantly less than that of BiVO₄. It may lead to the shielding of peaks of activated carbon by BiVO₄ in the composite. In terms of relative intensity there is no difference. AC only modified the surface of BiVO₄ and created defects in the crystal structure. The defects may become active centres for catalytic reaction. However, no peaks of unreacted by-products have been observed, suggesting that the material is highly pure. The average grain size of the BV and AC-BV nanoparticles was calculated using Scherrer formula

$$d = K\lambda / \beta \cos \theta \quad (2)$$

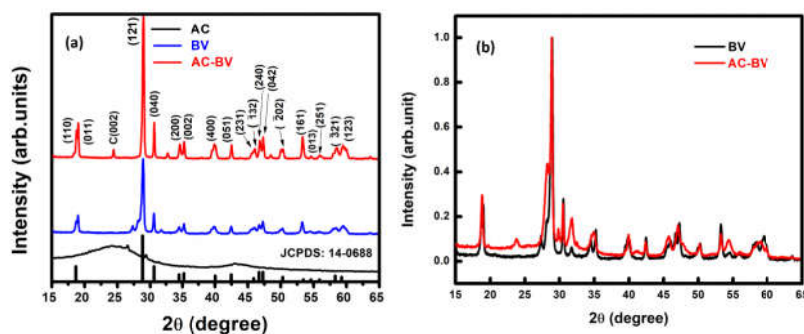


Figure 1: (a) Powder XRD patterns of BiVO₄ and AC-BiVO₄ nanoparticles, (b) Normalized intensity XRD plot of BiVO₄ and AC-BiVO₄ nanoparticles

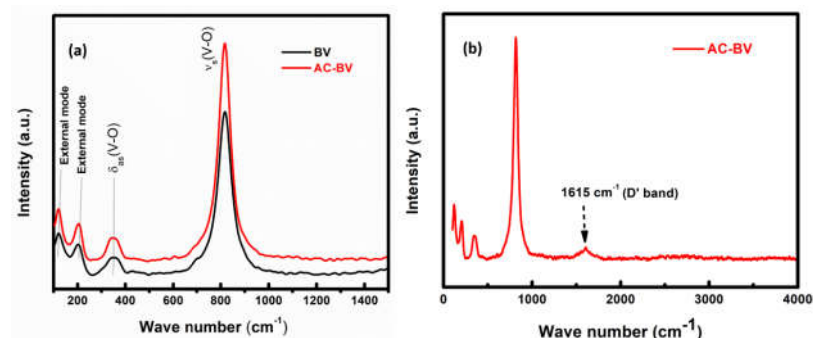


Figure 2: (a) Raman spectrum of BV and AC-BV samples, (b) Raman spectrum of AC-BV sample

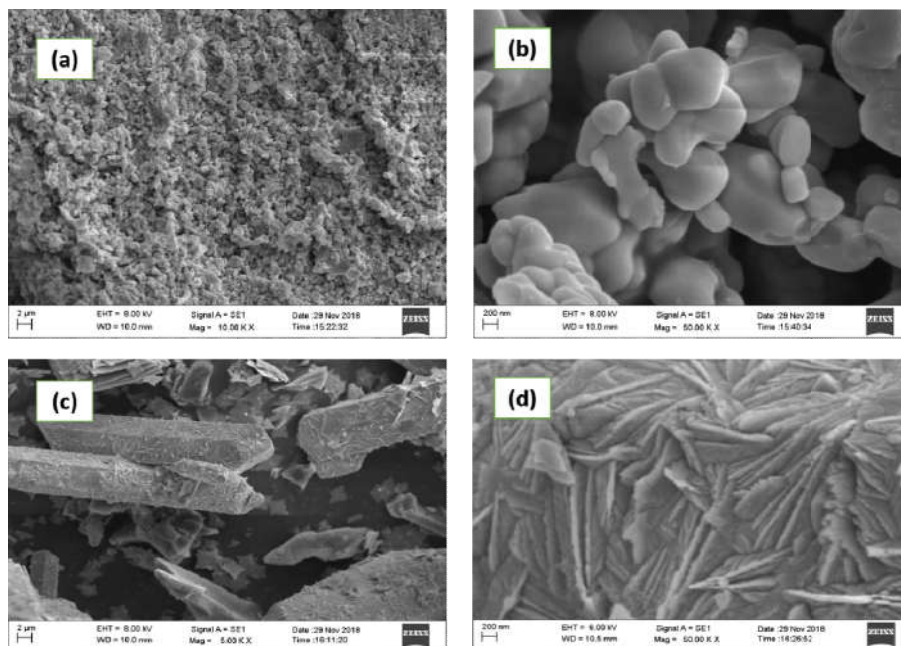


Figure 3: SEM micrographs at different magnifications of (a) & (b) BV nanoparticles, (c) & (d) AC-BV nanoparticles

Where d is the average crystallite size (nm), K is the shape factor, λ is the wavelength of Cu-K α (0.154 nm), β is the full width at half maxima; θ is the angle of diffraction. The average grain size of BV and AC-BV nanoparticles were found to be 21 nm and 17 nm respectively.

From the results of Raman spectrum, the composition of samples has been observed (Fig.2(a)). The lower wave number peaks located at 120 cm⁻¹ and 204 cm⁻¹ are assigned to external (rotation/translation) vibration modes [27]. The Raman band observed at 348 cm⁻¹ belongs to the bending mode of VO₄ tetrahedra. The most intense peak of 826 cm⁻¹ is attributed to the symmetric stretching vibration

mode of VO₄ tetrahedra [28]. All of these peaks matched well with vibrational modes of monoclinic scheelite structured BiVO₄, thus confirming the formation of monoclinic BiVO₄. A narrow peak found at 1615 cm⁻¹ as shown in Fig.2(b). This could be interpreted as a D' peak [29]. The structural distortion might be a reason for this [30].

Morphology

SEM micrographs (Fig. 3) illustrate the morphology of BV and AC-BV samples at various magnifications. The pure BV particles shows random morphology. However, upon

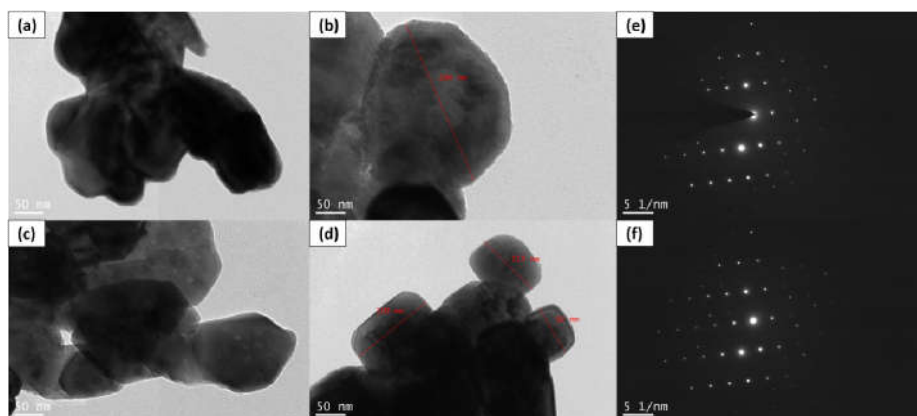


Figure 4: (a) & (b)- TEM images of BV nanoparticles, (c) & (d) - TEM images of AC-BV nanoparticles and (e) & (f) corresponding diffraction patterns

addition of AC there is a significant change in the morphology as well as particle agglomeration. The crystalline morphology is completely changed into a hexagonal shaped rod that is well composed of sharp edges. SEM micrographs of AC-BV also showed a porous morphology due to the existence of AC which influence to high porosity.

In addition, TEM analysis was carried out to provide more insight into the mesoporous BV and AC-BV nanoparticles as shown in Fig.4. TEM morphology highlights the change of spherical shaped BV nanoparticles to hexagonal nanotubes upon inclusion of AC which were interconnected and packed with pores, which attributed to the SEM micrographs. The Selected Area Electron Diffraction (SAED) diffraction spots shown in Fig.4(e) & 4(f) indicates that samples have high crystalline nature. The size of the BV and AC-BV nanoparticles are in the range of 290 nm and 118 nm respectively. Activated carbon act as a surfactant and it limits the agglomeration of particles. It may obstruct the continuity in bond formation. As a result, the particle size is reduced. The reduction in particle size usually leads to quadratic growth of the active surface area, which consecutively increases the number of external species reacting to the surface and leads to improved photocatalytic activity [31].

XPS Analysis

Pure BV and AC-BV nanoparticles have been characterised using XPS to get more insight into valence state and chemical composition [32]. In the XPS spectrum, the signals of Bi, V, C and O were determined. The survey spectrum of the BV and AC-BV photocatalysts shown in Fig. 5. The binding energy was referenced to the C1s peak at 284.8 eV. From the Fig. 6(a), two strong peaks were observed at 159.40 eV and 164.69 eV were attributed to Bi 4f_{7/2} and Bi 4f_{5/2} respectively, which indicates that Bi³⁺ cations are bismuth species in BV and AC-BV samples [33]. The chemical states of V species are displayed in Fig. 6(b). The binding energy at 517.04 eV and 524.28 eV are assigned to V 2p_{3/2} and V 2p_{1/2} evidencing the presence of V element as V⁵⁺ [34]. The chemical states of the atoms remain unchanged after modified with AC. From the O 1s (Fig.6(c)), the peak can be located at 530.24 eV which could be assigned for adsorbed oxygen. Upon the addition of AC improves the content of adsorbed oxygen and oxygen

vacancies that could render for enhancement of photocatalytic activity of BiVO₄ [35].

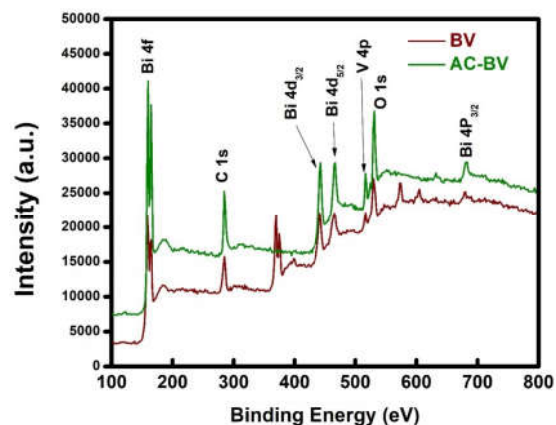


Figure 5: XPS survey spectrum of BV and AC-BV photocatalysts

Surface area analysis

A larger surface area has been demonstrated for the BV and AC-BV samples. It was key aspect for an effective photocatalyst in order to strengthen adsorption of reactants which in turn offer a higher amount of reaction sites [36]. The specific surface area and pore size distribution were studied using liquid nitrogen physisorption experiments. As shown in Fig. 7(a), the existence of hysteresis loops in the adsorption-desorption curves for BV and AC-BV nanoparticles belong to the type H4 hysteresis loops which specifies the presence of mesoporous structure in both samples [37]. As shown in Table 1 pure BV nanoparticles has a low specific surface area of 7.34 m²/g. However, due to the incorporation of AC the specific surface area of the nanoparticles increased drastically up to 68.10 m²/g, which is approximately 9 times greater than BV nanoparticles. Such difference can be attributed to small particle size and high crystal density of AC-BV photocatalyst. It was observed that as the surface area of the sample increases, the available number of active sites also increases on the photocatalyst surface leading to enhance the mobility of photo-induced electrons. Furthermore, it stimulates the active migration of charge carriers, resulting in a major improvement in photocatalytic efficiency [38].

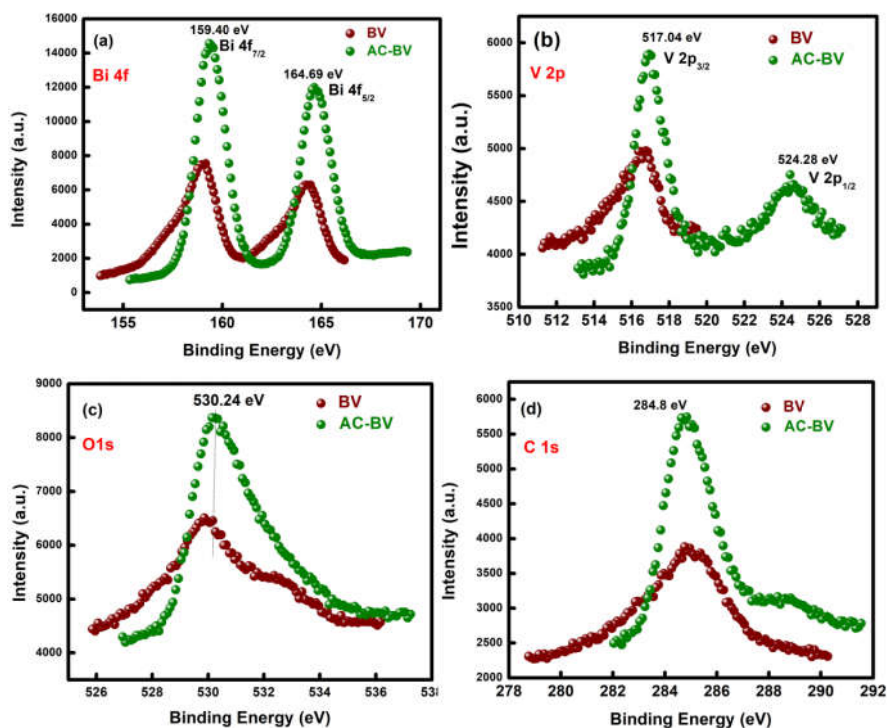


Figure 6: XPS spectra of (a) Bi 4f, (b) V 2p, (c) O 1s and (d) C 1s

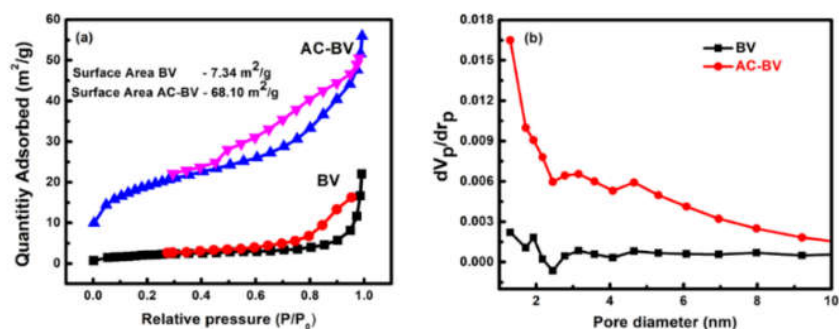


Figure 7: (a) BET nitrogen adsorption-desorption isotherms, (b) Pore size distribution of BV and AC-BV – BJH plot

Table 1: Parameters obtained from Nitrogen adsorption-desorption isotherms

Sample	Specific Surface Area	Pore Diameter	Pore Volume
BV	7.34 m ² /g	17.98 nm	0.04 cm ³ g ⁻¹
AC-BV	68.10 m ² /g	4.92 nm	0.08 cm ³ g ⁻¹

From the BJH pore size distribution (Fig. 7(b)), the mean pore diameter of BV nanoparticle is 17.98 nm and it is reduced to 4.92 nm of AC-BV nanoparticle. The volume of the pore was calculated from the amount of nitrogen adsorbed at maximum relative pressure of $P/P_0=0.99$, signifying that the pore size is quite large. The interaction between photocatalyst and organic compounds increases due to the larger specific surface area and higher pore volume of AC-BV nanoparticles. The specific surface area and pore volume are shown to increase as particle size is reduced. The increased surface area and smaller mesopores improves the number of active sites, which makes the particles with wide pore size distribution resulting in enhanced photocatalytic activity.

Optical properties

The optical properties of a semiconductor are more crucial for optimizing the electronic structure for the photocatalytic performance. UV-VIS DRS spectrum of

synthesized BV and AC-BV is depicted in Fig.8. The absorption spectra of both samples reveal that strong absorption in the visible region. The inclusion of AC evidently enhances the quantum efficiency of AC-BV material, that could lead to improved photocatalytic performance.

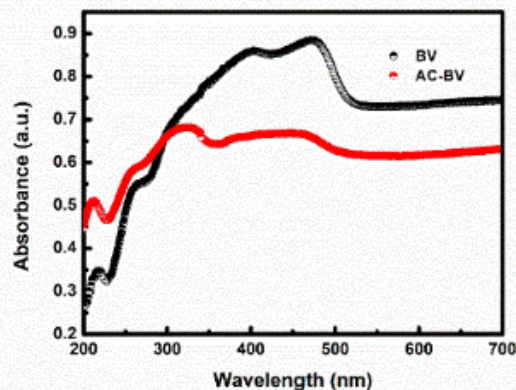


Figure 8: UV-Vis diffuse Reflectance spectra of hydrothermally synthesized BV and AC-BV nanoparticles

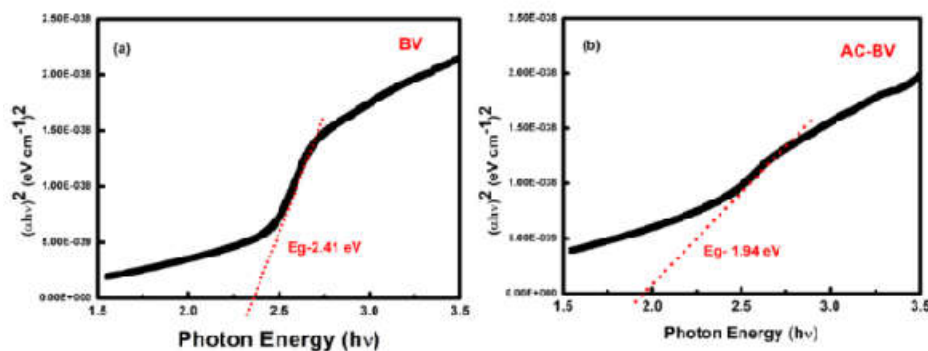


Figure 9: $(\alpha hv)^2$ versus photon Energy (hv) of (a) BV and (b) AC-BV photocatalysts

The bandgap corresponds to the optical absorption spectra of both materials were estimated by Tauc plot as shown in Fig.9(a) and 9(b). The value of bandgap energy of AC-BV particles is 1.94 eV, which is significantly lower than BV (2.41eV) nanoparticles. The decreasing bandgap of AC modified BiVO₄ increased the light absorption predominantly into visible region.

To assess the band position of BV and AC-BV photocatalysts, Mulliken's electronegativity theory has been generally adopted [39]. The VB and CB edge potentials of BV and AC-BV nanoparticles can be calculated by the following equations.

$$E_{VB} = \chi - E^c + [0.5 \times E_g] \quad (3)$$

$$E_{CB} = E_{VB} - E_g \quad (4)$$

Where E_{VB} is the valence band edge potential, E_{CB} is the conduction band edge potential, χ represents the absolute electronegativity of the semiconductor (i.e., the geometric mean of the constituent atoms), E^c is the standard electrode potential on the hydrogen scale ($E^c \sim 4.5$ eV) and E_g is the bandgap energy of the semiconductor. The VB potential can be calculated from the equation (3). Based on the bandgap positions, the estimated E_{VB} and E_{CB} of BV photocatalyst were determined to be 2.98 eV and 0.57 eV (vs NHE) respectively. Whereas, the E_{VB} and E_{CB} values of AC-BV are 1.56 eV and -0.38 eV (vs NHE) respectively.

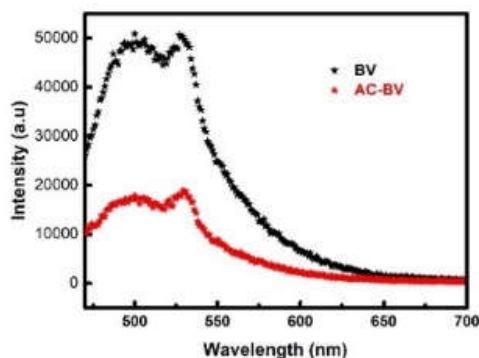


Figure 10: Photoluminescence spectra of BV and AC-BV nanoparticles at an excitation wavelength of 450 nm

The emission of PL in a semiconductor is usually related to the radiative photo-generated electron-hole recombination. The strong emission at 530 nm is perhaps a recombination of the hole created from the Bi 6s and O 2p hybrid orbitals and the electron produced from the V 3d orbitals. The electrons of BV nanoparticles are excited from

VB to CB by light irradiation, which leads to the formation of electron-hole pairs. The electrons produced can be transferred into AC that has high conductivity, and can be occupied for a great volume container of the electron. This might disrupt or inhibit electron-hole pair recombination [40]. Hence, lowest PL intensity of AC-BV indicates the lowest recombination of electron and hole (e^-/h^+) pairs. It was shown that in Fig. 10, AC-BV nanoparticles showed a significant amount of reduced emission intensity than BV nanoparticles, suggesting that a major suppression occurs in the recombination of charge carriers in AC-BV nanoparticles. During the photocatalytic process, the excited electrons are shifted from BiVO₄ to AC and thus greatly reducing the rate of recombination of photogenerated electron-hole pairs, that further enhances photocatalytic activity [41].

To further understand the recombination kinetics of photogenerated charge carriers, we examine the PL life time spectra (Fig. 11) of samples excited at 450 nm. The following equation was used to fit the decay curves using the tri-exponential function [42].

$$R(t) = A_1 e^{-t/\tau_1} + A_2 e^{-t/\tau_2} + A_3 e^{-t/\tau_3} \quad (5)$$

Where τ_1 , τ_2 , τ_3 are the decay components and A_1 , A_2 , A_3 are their relative amplitudes respectively. The average life time of charge carriers were calculated from the following equation [43]

$$\tau_{Avg} = \frac{\sum_{i=1}^n A_i \tau_i^2}{\sum_{i=1}^n A_i \tau_i} \quad (6)$$

The average life time of BV and AC-BV were found to be 21.45 ns and 90.70 ns respectively. In comparison to pure BiVO₄, the AC modified BiVO₄ sample has a longer life time. The recombination rate has decreased in AC-BV sample. It implies that trapped electrons will remain stay for longer, resulting in a large accumulation of electrons in the doped sample. Furthermore, AC-BV particles take longer time to recombine than pure particles, the photogenerated holes can be used to react with water molecules more effectively.

Photo degradation studies

Photodegradation performance of Rh-B has been carried out to investigate the photocatalytic activity of BV and AC-BV photocatalysts under direct sunlight irradiation and as shown in Fig.12 (a) & 12 (b). In the dark condition, Rh-B has been found to be more stable and there is no rate of degradation. As the duration of sunlight irradiation time

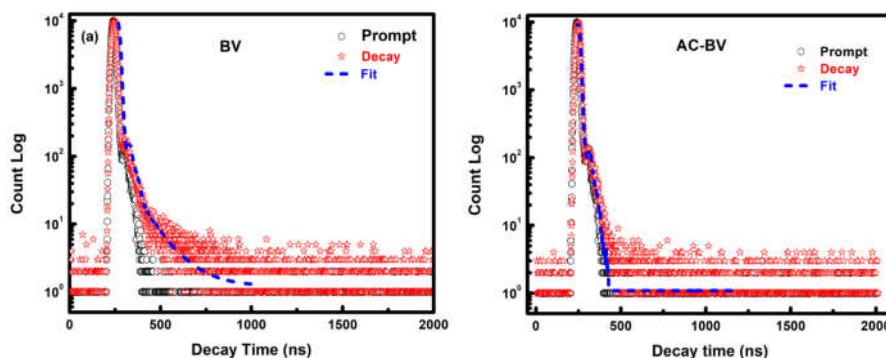


Figure 11: Life time decay observed in BV and AC-BV nanoparticles at excitation wavelength of 450 nm

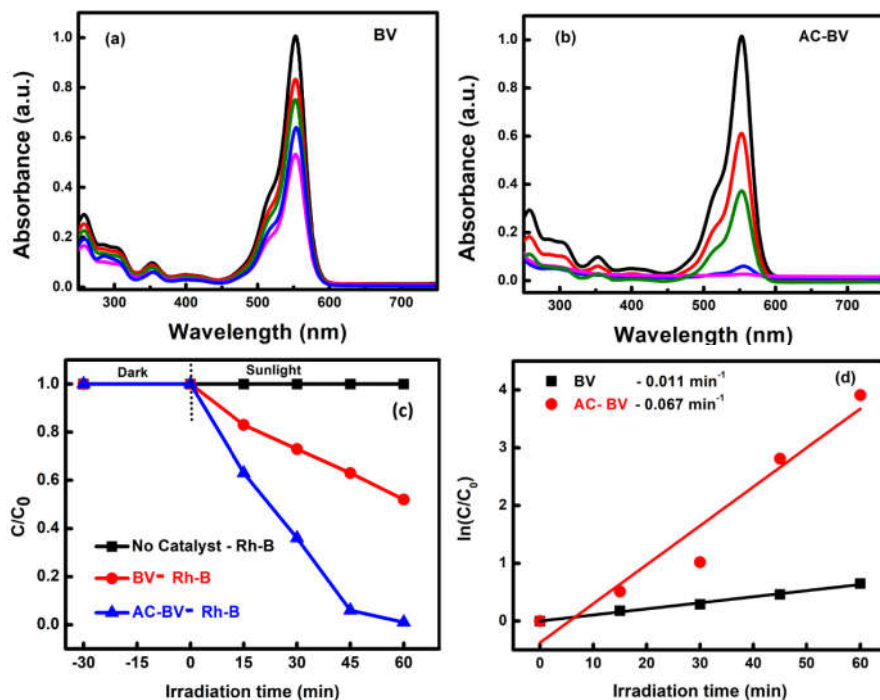


Figure 12: Time dependent photodegradation of Rh-B using (a) BV photocatalysts and (b) AC-BV photocatalysts under Sunlight irradiation, (c) Degradation profile (C/C_0) graph and (d) Photocatalytic reaction kinetics

Table 2: Overall photocatalytic activity of various AC-BiVO₄ nanocomposites

Photo Catalyst	Catalyst Amount	Synthesis Method	Amount of Dye	Light source	Irradiation Time	Deg. %	Reference
m-BiVO ₄ @ AC fibre	0.1 g	Solvothermal	5mg/L	Visible light	180 min	86%	[44]
BiVO ₄ -AC fibre	0.2g	Hydrothermal Immobilization	40mg/L	1000W Xe Arc Lamp	4 hours	90%	[47]
m-BiVO ₄ hollow sphere/AC fibres	0.33g	Hydrothermal	-	Visible light	2 hours	78%	[48]
AC-BiVO ₄	0.05 g	Hydrothermal	10 mg/L	Sunlight	60 min	98%	Present work

increase, the colour of the solution will be disappeared. It was disrupted due to the breakdown of Rh-B. This occurs owing to the adsorption of Rh-B dye on the surface of the catalyst and degradation of dye by the photocatalysts [44]. The degradation rate is nearly 47% for BV photocatalyst and 98% for AC-BV photocatalyst within 60 minutes of sunlight illumination. The enhanced Rh-B degradation percentage reported for the AC-BV composite is owing to the presence of AC in the composite, as evidenced by the

degradation performance, which shows that increasing the surface area attracts more dye molecules. Another factor that is responsible for the increased dye degradation property would be the bandgap narrowing. The narrowing of the bandgap typically involves the scattering of CB minimum and VB maximum which accelerates the photo generated electrons and holes [45].

Fig.12(c) shows the effects of BV and AC-BV photocatalysts on Rh-B at different time intervals. It clearly shows that the

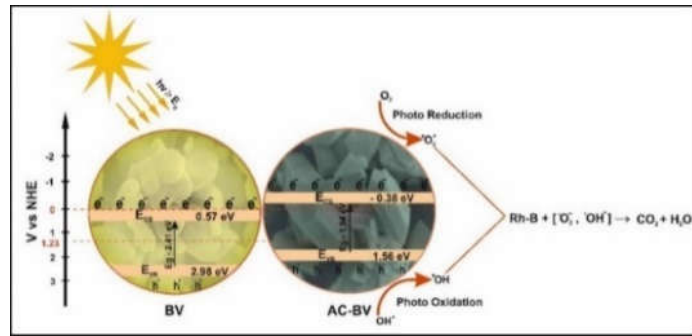


Figure 13: Schematic illustration of the mechanism of degradation over AC-BV photocatalyst under sunlight irradiation

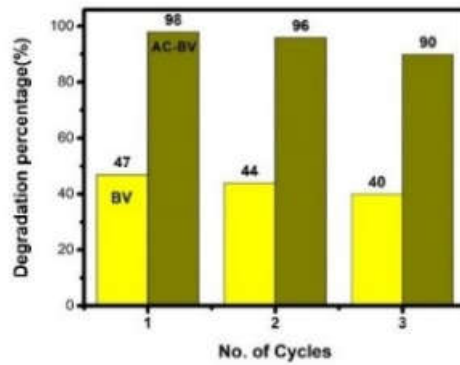


Figure 14: Recyclability of BV and AC-BV samples for the degradation of Rh-B under the Sunlight irradiation

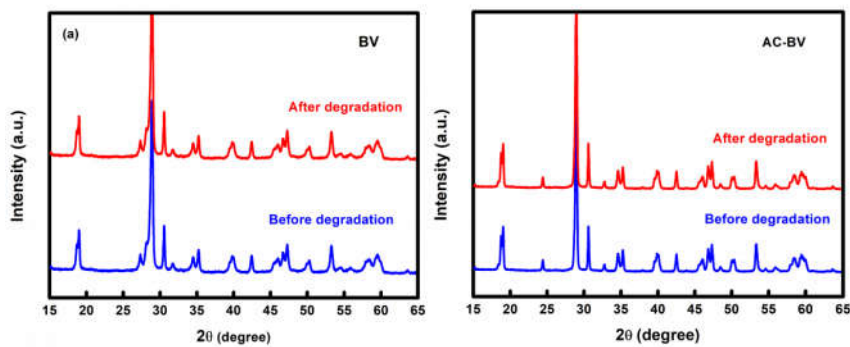


Figure 15: XRD patterns of BV and AC-BV before and after successful cycles of photocatalytic dye degradation

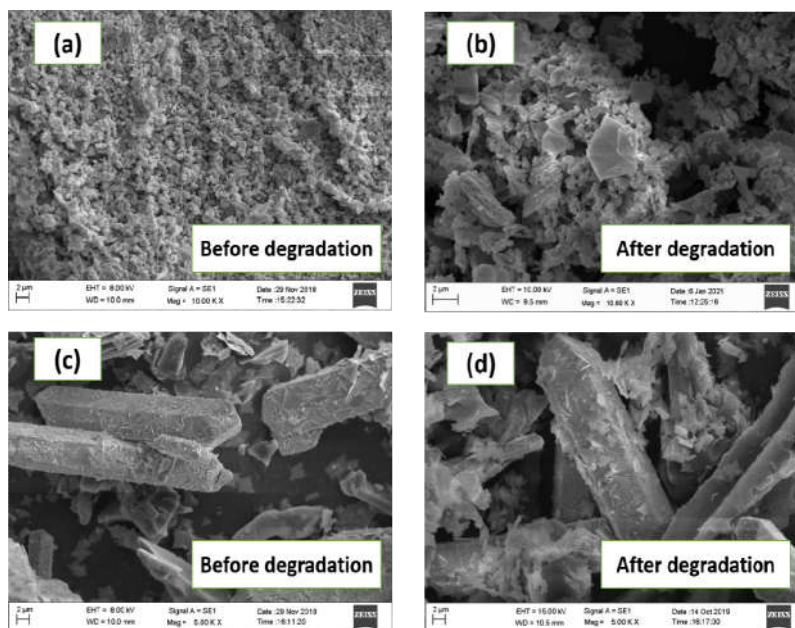


Figure 16: SEM micrographs of BV and AC-BV after three recycles

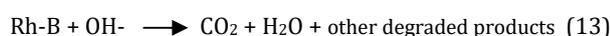
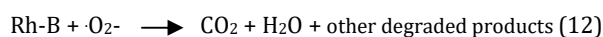
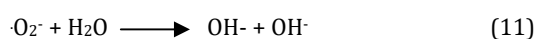
degradation rate increases for AC-BV composite material. This might be due to the increase in active sites and reduced recombination rate. The pseudo-first order kinetic model has been applied to obtain the rate constant (k), to examine the reaction kinetics of the Rh-B degradation. It was calculated by using the following equation [46].

$$\ln (C_0/C) = k t \quad (7)$$

Where, C₀ represents the initial concentration of Rh-B solution, C represents concentration of Rh-B under irradiation of light at given time and k is the observed first order rate constant. The reaction rate constant has been calculated from the slope of the plots (Fig.12(d)) drawn between C₀/C and irradiation time (t). The rate constant (k) of Rh-B degradation for AC-BV (k- 0.067 min⁻¹) photocatalyst is higher than that of BV (k- 0.011 min⁻¹) photocatalyst. Table 2 describes the overall photocatalytic activity of various AC-BiVO₄ nanocomposites.

Proposed Photodegradation Mechanism

A probable Sunlight driven photocatalysis mechanism is proposed as follows. The BV nanoparticles are exposed to direct sunlight, photogenerated e⁻/h⁺ pairs were formed. The photogenerated electrons are excited from VB to the CB, thereby leaving positively charged holes in the VB. The photoinduced electrons in the AC-BV nanoparticles are captured by O₂, prompting the formation of superoxide radical (O₂⁻). Simultaneously, the holes in the VB react with water molecules to produce a hydroxyl radical (OH[•]). The generated superoxide radical (O₂⁻) further reacts with H₂O to create more hydroxyl radicals. The superoxide radicals and hydroxyl radicals are responsible for the degradation of organic pollutants. The reactions are involved in the photocatalytic degradation of Rh-B could be summarized from the following equations.



Based on the energy band positions, the possible degradation mechanism of AC-BV composite as illustrated in Fig.13. The interaction of BV nanoparticles with AC well formed a heterojunction between them. At first, the organic molecules are adsorbed on the surface of AC with BV-AC heterojunction [49]. In the case of pure BV, the particles are mostly agglomerated, resulting in a higher proportion of recombined e⁻-h⁺ pairs and further exhibit lower photocatalytic activity. Whereas, the AC modified BV showed improved activity that is attributed to the adverse effects of drastically low recombination due to the uniform distribution of particles without agglomeration. In addition to that AC-BV photocatalysts have improved surface area by enhancing the dye adsorption properties by providing more adsorption sites that facilitates rapid degradation compared to BV photocatalysts. The BV nanoparticles act as a photoactive centre when sunlight is illuminated, thus producing photogenerated charge carriers. These charge

carriers further create superoxide radicals and hydroxyl radicals to decompose the organic compounds.

Photostability and Reproducibility test

The recyclability of photocatalysts defines its importance in practical applications. In order to evaluate the recycling ability of BV and AC-BV photocatalysts, repeated photocatalytic studies have been conducted for three cycles as shown in Fig.14. The used photocatalysts demonstrated good stability after three consecutive cycles that further proves its reusability. Furthermore, there is no discernible change in the XRD patterns of BV and AC-BV in Fig.15. after three cycles of photocatalytic dye degradation. The morphology of the as prepared photocatalysts after photocatalytic recycling analysis was monitored by SEM. After three runs the morphology of BiVO₄ and AC-BiVO₄ not varied much as compared to a fresh sample (Fig.16).

Conclusions

Photocatalytic degradation of Rh-B on AC modified BiVO₄ nanoparticles under direct sunlight irradiation has been examined. We have proposed a simple hydrothermal method to prepare AC-BiVO₄ nanoparticles. The synthesized pure BiVO₄ and AC-BiVO₄ materials demonstrated a monoclinic scheelite structure which has been confirmed by XRD. The inclusion of porous AC is considerably enhanced the photocatalytic activity by providing a greater number of active sites for dye adsorption and an extended visible region by narrowing the bandgap from 2.4 eV to 1.9 eV. A synthesized AC-BiVO₄ nanoparticles shows enhanced photocatalytic activity than pure BV nanoparticles. The efficiency of photocatalytic degradation of Rh-B significantly improves to 98% for AC-BiVO₄ composite. This AC incorporated BiVO₄ photocatalyst would be an excellent material for environmental remediation and enable the natural sunlight as an alternative driving energy.

Acknowledgments

This work was financially supported by Anna University in the form of Anna Centenary Research Fellowship (ACRF) from the Centre for Research, Anna University Chennai.

Declaration of competing interest

The authors declare that they have no known competing financial interests or personal relationships that could have appeared to influence the work reported in this paper.

References

1. Kailian Zhang, Man Zhou, Changlin Yu, Kai Yang, Xiaoxia Li, Wenxin Dai, Jie Guan, Qing Shu, Weiya Hu, Construction of S-scheme g-C₃N₄/ZrO₂ heterostructures for enhancing photocatalytic disposals of pollutants and electrocatalytic hydrogen evolution, *Dyes Pigm.*, 2020, 180, 1-13.
2. Yi-Hsuan Chiu, Tso Fu Mark Chang, Chun-Yi Chen, Mastro Sone, Yung-Jung Hsu, Mechanistic insights into photodegradation of organic dyes using heterostructure photocatalysts, *Catalysts*, 2019, 9, 1-32.
3. Babatunde A. Koiki, Benjamin O. Orimolade, Gbenga M. Peleyeju, Omatayo A. Arotiba, Rapid and template-free synthesis of copper(I) oxide-graphitic carbon nitride heterojunction for photocatalytic degradation of orange II dye in water, *Solid State Sci.*, 2019, 97, 1-8.
4. Wanyin Ge, Siyi Jiao, Meimei Xu, Jindou Shi, Zhe Chang, Tricylphosphine (TOP)- free synthesis of TiSe₂ plates for enhanced photocatalytic degradation performance of Rhodamine B dyes, *Solid State Sci.*, 2020, 103, 1-8.

5. Yuvaraj M. Hunge, Anuja A. Yadav, Babasaheb M. Mohit, Basics of Photocatalysis and Different Strategy for Enhancing the Photocatalytic Efficiency, *Am J App Sci.*, 2020, 12, 265-268.
6. Yiou Wang, Fabrizio Silveri, Mustafa K. Bayazit, Qiushi Ruan, Yaomin Li, Jijia Xie, C. Richard A. Catlow, Junwang Tang, Bandgap engineering of organic semiconductors for highly efficient photocatalytic water splitting, *Adv Energy Mater.*, 2018, 8, 1-10.
7. Adalagere Somashekar Manjunatha, Nyathappa Siddagamma Pavithra, Shivana Marappa, Shivappa Adarakatti Prashanth, Ganganagappa Nagaraju, Puttuswamy, Green synthesis of flower like BiVO₄ nanoparticles by solution combustion method using lemon (Citrus limon) juice as a fuel: photocatalytic and electrochemical study, *Chemistry Select*, 2018, 3, 13456-13463.
8. Caamila S. Ribeiro, Milena D. Brandestini, Celso C. Moro, Marla A. Lansarin, A fair comparison between bismuth catalysts for application in photodegradation under visible and solar light, *Braz J Chem Eng.*, 2018, 36, 201-208.
9. A. Malathi, J. Madhavan, Muthupandian Ashokkumar, Prabhakarn Arunachalam, A review on BiVO₄ photocatalyst: Activity enhancement methods for solar photocatalytic applications, *Appl Catal A: Gen.*, 2018, 555, 47-74.
10. Chan Qin, Hongru Liao, Feiyang Rao, Junbo Zhong, Jianzhang Li, One-pot hydrothermal preparation of Br-doped BiVO₄ with enhanced visible-light photocatalytic activity, *Solid State Sci*, 2020, 105, 1-9.
11. Junlong Zhang, Yan Lu, Lei Ge, Changcun Han, Yujing Li, Yangqin Gao, Songsong Li, Hao Xu, Novel AuPd bimetallic alloy decorated 2D BiVO₄ nanosheets with enhanced photocatalytic performance under visible light irradiation, *Appl Catal B*, 2017, 204, 385-393.
12. W.Z. Wang, Shan Meng, Miao Tan, L.J. Jia, Y.X. Zhou, Shuang Wu, X.W. Huang, Y.J. Liang, H.L. Shi, Synthesis and the enhanced visible-light-driven photocatalytic activity of BiVO₄ nanocrystals coupled with Ag nanoparticles, *Appl Phys A*, 2015, 118, 1347-1355.
13. Chunli Song, Zhanbin Jin, Fengyan Li, Miaomiao Zhen, Lu Xi, Lin Xu, Enhanced photocatalytic performance of bismuth vanadate assisted by polyoxometalates and phthalocyanine, *New J Chem.*, 2018, 42, 19678-19684.
14. Duangdao Chanhei, Auppatham Nakaruk, Wilawan Khanitchaidecha, Panatda Jannoey, Sukon Phanichphant, Adsorption and photocatalytic processes of mesoporous SiO₂-coated monoclinic BiVO₄, *Front Chem.*, 2018, 6, 1-7.
15. Deqiang Zhao, Wenwen Wang, Wenjuan Zong, Shimin Xiong, Qian Zhang, Fangying Ji Yuan Xu, Synthesis of Bi₂S₃/BiVO₄ heterojunction with a one-step hydrothermal method based on pH control and the evaluation of visible-light photocatalytic performance, *Materials*, 2017, 10, 1-15.
16. Dang Trunk Tri Trinh, Duangdao Chanhei, Kantapat Chansaenpak, Wilawan Khanitchaidecha, Auppatham Nakaruk, Photocatalytic degradation of organic dye over bismuth vanadate-silicon dioxide-graphene oxide nanocomposite under visible light irradiation, *J Aust Ceram Soc.*, 2020, 56, 1237-1241.
17. Youji Li, Feitai Chen, Rongan He, Yingchun Wang, Ningmei Tang, Chapter 24 - Semiconductor Photocatalysis for Water Purification, In *Micro and Nano Technologies, Nanoscale Materials in Water Purification*, 2019, 689-705.
18. Juan Matos, Po S. Poon, Ricmary Montana, Romina Romero, Gustavo R. Goncalves, Mignel A. Schettino Jr, Edson C. Passamani, Jair C.C. Freitas, Photocatalytic activity of P-Fe/activated carbon nanocomposites under artificial solar irradiation, *Catal.*, 2019, 356, 1-15.
19. Xiaoqing Chen, Zhansheng Wu, Zhenzhen Gao, Bang-Ce Ye, Effect of different activated carbon as carrier on the photocatalytic activity of Ag-N-ZnO photocatalyst for methyl orange degradation under visible light irradiation, *Nanomaterials*, 2017, 7, 1-18.
20. Xiaojing Wang, Yafei Liu, Zhonghua Hu, Yujuan Chen, Wei Liu, Guohua Zhao, Degradation of methyl orange by composite photocatalysts nano-TiO₂ immobilized on activated carbons of different porosities, *J Hazard Mater.*, 2009, 169, 1061-1067.
21. Amel Taha, Melek Ben Aissa, Enshirah Da'na, Green Synthesis of an Activated Carbon-Supported Ag and ZnO Nanocomposite for Photocatalytic Degradation and its Antibacterial Activities, *Molecules*, 2020, 25, 1-18.
22. Steplinpaulselvin. S, Ganesh kumar. A, Sarala. L, Rajaram. R, Sthiyana. A, Princy Merlin. J, Sharmila Lydia. I, Photocatalytic Degradation of Rhodamine B Using Zinc Oxide Activated Charcoal Polyaniline Nanocomposite and its Survival Assessment Using Aquatic Animal Model, *ACS Sustainable Chem Eng.*, 2018, 6, 258-267.
23. Baolin Xing, Changliang Shi, Chuanxian Zhang, Guiyun Yi, Lunjian Chen, Hui Guo, Guangxu Huang, Jianliang Cao, Preparation of TiO₂/activated carbon composites for photocatalytic degradation of RhB under UV light irradiation, *J Nanomater.*, 2016, 3, 1-11.
24. Su-Hua Chen, Yong-Siang Jiang, Hsin-yu Lin, Easy synthesis of BiVO₄ for photocatalytic overall water splitting, *ACS Omega*, 2020, 5, 8927-8933.
25. Vasudha Hasija, Pankaj Raizada, Anita Sudhaik, Pardeep Singh, Vijay Kumar Thakur, Aftab Aslam Parwaz Khan, Fabrication of Ag/AgI/WO₃ heterojunction anchored P and S co-doped graphitic carbon nitride as a dual Z scheme photocatalyst for efficient dye degradation, *Solid state sci.*, 2020, 100, 1-9.
26. Shigeru Ikeda, Takatoku Kawaguchi, Yui Higuchi, Naoto Kawasaki, Takashi Harada, Mikas Remeika, Muhammad M Islam, Takeaki Sakurai, Effects of zirconium doping into a monoclinic scheelite BiVO₄ crystal on its structural, photocatalytic and photoelectrochemical properties, *Front Chem.*, 2018, 6, 1-6.
27. Chunjing Shi, Xiaoli Dong, Jiawei Wang, Xiuying Wang, Hongchao Ma, Xiufang Zhang, Interfacial defect engineering over fusiform bismuth vanadate photocatalyst enables to excellent solar-to-chemical energy coupling, *RSC Adv.*, 2017, 7, 26717-26721.
28. Deqiang Zhao, Wenjuan Zong, Zihong Fan, Shimin Xiong, Mao Du, Tianhui Wu, Yue Wen Fang, Fangying Ji, Xuan Xu, Synthesis of carbon-doped BiVO₄@multi-walled carbon nanotubes with high visible light absorption behavior and evaluation of their photocatalytic properties, *Cryst Eng Comm.*, 2016, 18, 9007-9015.
29. N. Shimodaria, A. Masui, Raman spectroscopic investigations of activated carbon materials, *J Appl Phys.*, 2002, 92, 901-909.
30. R. Vidano, D.B. Fischbach, New lines in the Raman spectra of carbons and Graphite, *J Am Ceram Soc.*, 1978, 61, 13-17.
31. B.P. Reddy, V. Rajendar, M.C. Shekar, S.H. Park, Particle size effects on the photocatalytic activity of BiFeO₃ particles, *Dig J Nanomater Biostruct.*, 2018, 13, 87-95.
32. Ankush Chauhan, Ritesh Verma, Swati Kumari, Anand Sharma, Pooja Shandilya, Yiangkai Li, Khalid Mujasam Batoo, Ahamad Imran, Sauralah Kulshrestha, Rajesh Kumar, Photocatalytic dye degradation and antimicrobial activities of Pure and Ag-doped ZnO using Cannabis sativa leaf extract, *Sci Rep.*, 2020, 10, 1-16.
33. Chhabil Regmi, Dipesh Dhakal, Soo Wahn Lee, Visible-light-induced Ag/BiVO₄ semiconductor with an enhanced photocatalytic and antibacterial performances, *Nanotechnology*, 2018, 29, 1-17.
34. Rania E. Adam, Hatim Alnoor, Galia Pozina, Xianjie Liu, Magnus Willander, Omer Nur, Synthesis of Mg-doped ZnO NPs via a chemical low-temperature method and investigation of the efficient photocatalytic activity for the degradation of dyes under solar light, *Solid State Sci.*, 2020, 99, 1-38.
35. F. Li, L. Zhang, X. Chen, Y.L. Liu, S.G. Xu, S.K. Cao, Synergistically enhanced photocatalytic reduction of CO₂ on N-Fe co doped BiVO₄ under visible light irradiation, *Phys Chem Chemphys.*, 2017, 19, 21862-21868.
36. Xialong Wang, Min Xu, Lu Liu, Yan Cui, Hansong Geng, Hongli Zhao, Bo Liang, Jingkai Yang, Effects specific surface area and oxygen vacancy on the photocatalytic properties of mesoporous F doped SnO₂ nanoparticles prepared by

- hydrothermal method, *J Mater Sci Mater in Electron.*, 2019, 30, 16110-16123.
37. Youju Shu, Shengrong Yan, Kaijie Dong, Jiwei Chen, Preparation of novel mesoporous photocatalyst Bi₄O₅Br₂/SBA-15 with enhanced visible light catalytic activity, *Open J Appl Sci.*, 2018, 8, 532-544.
 38. Taiping Xie, Hui Li, Chenglun Liu, Jun Yang, Tiancun Xiao, Longjun Xu, Magnetic Photocatalyst BiVO₄/Mn-Zn ferrite/Reduced Graphene Oxide: Synthesis Strategy and its Highly Photocatalytic Activity, *Nanomaterials*, 2019, 8, 1-13.
 39. Tauseef Munawar, Faisal Mukhtar, Muhammad Shahid Nadeem, Muhammad Riaz, Muhammad Naveed ur Rahman, Khalid Mahmood, Murtaza Hasan, M.I. Arshad, Fayyaz Hussain, Altaf Hussain, Faisal Iqbal, Novel photocatalyst and antibacterial agent; direct dual Z-scheme ZnO-CeO₂-Yb₂O₃heterostructured nanocomposite, *Solid state sci.*, 2020, 109, 1-14.
 40. Radwa A. Elsalamony, EnasAmdeha, Nagwa A. Badawy, Salwa A. Ghoneim, Ahmed M. Al-Sabag, Visible light sensitive activated carbon-metaloxide (TiO₂, WO₃, NiO, and SnO) nano-catalystsfor photo-degradation of methylene blue: a comparative study, *Toxicol Environ Chem.*, 2018, 100, 100143-100156.
 41. Xiatong Wang, Jianqing Zhou, Shuo Zhao, Xiao Chen, Ying Yu, Synergistic effect of adsorption and visible-light photocatalysis for organic pollutant removal over BiVO₄/carbon sphere nanocomposites, *Appl Surf Sci.*, 2018, 453, 394-404.
 42. R.Janani, G.SudhaPriyanga, Santosh Behara, Ambrose Ashwin Melvin, A.R.M.Shaheer, Tiju Thomas, BernardshawNeppolian, Shubra Singh, Enhanced solar light driven hydrogen generation and environment remediation through Nd incorporated ZnInS₄, *Renew Energy*, 2020, 162, 2031-2040.
 43. Zhenyi Zhang, Kuichao Liu, Zhiqing Feng, Yanan Bao, Bin Dong, Hierarchical sheet on sheet ZnIn₂S₄/gC₃N₄ heterostructures with highly efficient photocatalytic H₂ production based on photoinduced interfacial charge transfer. *Sci Rep.*, 2015, 6, 1-10.
 44. Aimen Saleem, Toheed Ahmed, Muhammad Ammar, Hongling Zhang, Hong-bin Xu, Romana Tabassum, Direct growth of m-BiVO₄@carbon fibers for highly efficient and recyclable photocatalytic and antibacterial applications, *J Photochem Photobiol B.*, 2020, 213, 1-11.
 45. Xiaohui Ji, Jiu-Fu Lu, Qin Wang, Dan Zhang, Impurity doping approach on bandgap narrowing and improved photocatalysis of Ca₂Bi₂O₅, *Powder Technol.*, 2020, 376, 708-723.
 46. Qingming Meng, Zhiquan Yin, Juan Jiang, Wenna Liu, Electrospun nanofibers of Pd-doped α-Bi₂O₃ for enhancing photocatalytic denitrification of fuel oil under visible light, *Mat Sci Semicon Proc.*, 2020, 121, 1-8.
 47. Chencheng Zhang, Pingfang Han, Xiaoping Lu, Qinghui Mao, Jiangang Qu, Ya Li, Preparation and photocatalytic activity characterization of activated carbon fiber-BiVO₄ composites, *RSC Adv.*, 2018, 8, 24665-24672.
 48. Toheed Ahmed, Hong-ling Zhang, Hong-bin Xu, Yi Zhang, m-BiVO₄ hollow spheres coated on carbon fiber with superior reusability as photocatalyst, *Colloid Surface A.*, 2017, 531, 213-220.
 49. Sagar Kande, UdhavGhoshir, Jayashree Khedhar, Anil Gambhire, Cadmium Sulfide Loaded Activated Carbon: An Efficient, Solar Light Driven Photocatalyst for Rhodamine B Dye Degradation, *Orient J Chem.*, 2019, 35, 1037- 1044.

